A Novel Miniaturized Dual Band Slotted Monopole Antenna for WLAN and WiMAX Applications

**Omaima Benkhadda[1, *], Mohamed Saih[1], Kebir Chaji[1],
Sarosh Ahmad[2, 3], and Abdelati Reha[4]**

Abstract—This study presents a novel design for a dual-band antenna that is compact, efficient, and suitable for both WLAN and WiMAX applications. The antenna features a circular patch with a Hilbert fractal structure and a coplanar waveguide feed line, resulting in a compact size of $24 \times 34 \times 1.6 \, \text{mm}^3$. By utilizing a Hilbert fractal slot and defected ground structure, the antenna can operate in two frequency bands, 2.39–2.47 GHz and 3–6.32 GHz, providing coverage for the desired WiMAX and WLAN bands. The experimental results demonstrate acceptable gains and high efficiency at the resonant frequencies, along with omnidirectional radiation patterns in the H-plane and bidirectional patterns in the E-plane. Notably, this design offers a nearly 50% reduction in size compared to comparable antennas and higher gain, representing a significant contribution to the field of dual-band antenna design.

1. INTRODUCTION

With the advancement of wireless communication technology, microstrip patch antennas have aroused significant interest because of their reduced size, low weight, simplicity of manufacturing, and integration. It also offers an effective strategy to reach multiband performance on a single device, which helps access a variety of wireless services such as WLAN, WiMAX, and others that are generally used in wireless communication systems [1–5].

In the literature, numerous approaches exist for developing multiband and wideband antennas for WLAN and WiMAX bands. Among them is the use of slots in radiators, fractal structure, and metamaterial. In [6], a monopole antenna powered by coplanar waveguide (CPW) fed with a rectangular slot carved into the ground was developed to generate three bands at 2.4, 3.5, and 5.5 GHz. The authors in [3] reported a slotted monopole antenna with two E and inverted T-stubs for quad-band applications. However, it had a large surface area of $44 \times 56 \times 1.6 \, \text{mm}^3$. The authors in [7] developed a slotted CPW-fed Cantor fractal antenna with an overall size $42 \times 50 \times 1.6 \, \text{mm}^3$, and the designed antenna is operational at the frequencies 2.6, 5.3, 8, and 10 GHz. However, it did not resonate around 3.5 and 3.6 GHz. In [8], an A-shaped antenna powered by a coaxial probe fed was designed, and it achieved broadband of 4 GHz. In [9], a fork-shaped monopole antenna was designed to achieve dual-band operations. In [10], an F-shaped monopole antenna powered by an asymmetric coplanar strip was suggested to achieve four bands. After that, an asymmetric quad-band monopole antenna was introduced in [11]. A circular slot monopole antenna was presented in [12] to generate two bands operating at 3.5 and 5.8 GHz. However, it did not cover the WLAN and WiMAX bands around 2.4 GHz. A fractal antenna with CSSR for multiband applications was presented in [13]; however, it occupied a large size of $60 \times 60 \times 1.6 \, \text{mm}^3$. A

* Corresponding author: Omaima Benkhadda (oabenkhadda@gmail.com).
[1] Microelectronics, Embedded Systems and Telecommunication Team, Faculty of Sciences and Technology, Sultan Moulay Slimane University, Beni Mellal 23000, Morocco. [2] Department of Electrical Engineering and Technology, Government College University Faisalabad (GCUF), Faisalabad, Pakistan. [3] Department of Signal Theory and Communications, Universidad Carlos III de Madrid, Leganés 28911, Madrid, Spain. [4] Laboratory of Innovation in Management and Engineering for the Enterprise (LIMIE), ISGA Marrakech 40000, Marrakech, Morocco.

monopole antenna with defected ground structure was designed in [14]. However, the designed antenna had an overall size of $50 \times 50 \times 1.6\,\mathrm{mm}^3$, and it did not cover the WLAN and WiMAX bands around 3.6 GHz. According to [15], a meander line antenna was designed to achieve four bands; however, it did not shield the band around 3.5 GHz. A monopole-fed double folded dipole antenna is proposed in [16]. It provides a quad-band. However, it had a large size of $110 \times 68 \times 1.6\,\mathrm{mm}^3$, and it did not cover the bands around 5.5 and 5.8 GHz. In [17], a W-shaped antenna with a defected ground structure (DGS) was designed to resonate around 0.9 and 2.45 GHz. However, it had a large size $40 \times 78 \times 0.254\,\mathrm{mm}^3$. In [18], a monopole antenna inspired from Chinese window was presented to achieve four bands around 1.6, 2.35, 3.8, and 5.85 GHz. However, it had a large surface area of $85 \times 70 \times 1.6\,\mathrm{mm}^3$. In [19], a planar antenna with two F-shaped resonators powered by coaxial probe feed was introduced to generate three bands at 1.8, 3.5, and 5.8 GHz. However, it had a large size, and it did not shield the band around 2.4 GHz. In [20], a complementary stacked microstrip antenna with a modified Minkowski fractal shaped defect achieved a wide bandwidth.

References [21–25] present antennas based on metamaterial techniques for WLAN and WiMAX applications. The authors in [21] developed a CPW-fed metamaterial antenna to generate three bands at 2.4, 3.5, and 5.5 GHz. [22] reported a circular shape split ring resonator (SRR) fed by CPW technique for WLAN and WiMAX bands. According to [23], a triangular antenna with a triangular SRR was proposed. In [24], an SRR antenna was developed for resonating around 2.45, 4.5, 6, and 9 GHz. In [25], a slotted rectangular antenna with an SRR array was developed for resonating at 2.4, 3.5, and 5.5 GHz frequencies.

This work designs a novel dual-band circular antenna consisting of a Hilbert fractal slot and DGS for WLAN and WiMAX applications. The designed antenna provides two bands, the first band from 2.39 to 2.47 GHz with a resonant frequency of 2.45 GHz and the second band from 3 to 6.32 GHz with two operating frequencies of 3.6 and 5.7 GHz. The first band is achieved by etching the second iteration into the circular radiator. Moreover, the second band is realized using a CPW feed line and DGS. The proposed antenna provides an acceptable gain and high radiation efficiency about 1.7/2.7/4.02 dBi and 97/95/96%, respectively, at the operating frequencies 2.45/3.6/5.7 GHz. Additionally, the E- and H-planes radiation patterns are omnidirectional. The remainder of this paper is as follows. The antenna geometry and design evolution process are detailed in the first section of this paper. Section 2 presents a parametric investigation of antenna dimensions. In section 3, the results acquired by the simulation and measurement are discussed. The work's conclusion is presented in the final section.

2. ANTENNA DESIGN METHODOLOGY

2.1. Geometry of the Miniaturized Dual-Band Antenna

Figure 1 exhibits the geometry of the designed antenna. Its construction comprises a circular radiating element loaded with the iteration number two of Hilbert fractal slot. As illustrated in Fig. 1, the suggested antenna is excited by a CPW technique. A microstrip line of width Wf makes up the transmission line (TL), and the gap g separates the TL. The ground plane is set to achieve a $50\,\Omega$ in the input impedance. The developed antenna is mounted on a 1.6-mm-FR-4 epoxy substrate with a relative permittivity ε_r of 4.4 and a loss tangent of 0.025. The substrate length and width define the antenna's overall size, L_{sub} and W_{sub}, which are 34 mm and 24 mm, respectively.

It should be highlighted that the designed antenna has a miniaturized size for the use in compact devices. A parametric investigation and the evolution process of the proposed antenna were utilized to evaluate its performance and identify its optimal parameters, as shown in Table 1. The suggested antenna was developed and performed using CST MWS software.

2.2. Design Process of the Miniaturized Dual-Band Antenna

To have a better comprehension of the suggested antenna evolution, Fig. 2 depicts its evolution steps from the basic circular antenna to the structure of the investigated antenna. A CPW-feed powers a circular radiator at the beginning of the antenna evolution process. To create the final geometry, the iterations one and two of Hilbert fractal slots are loaded into the patch. Furthermore, two similar slots
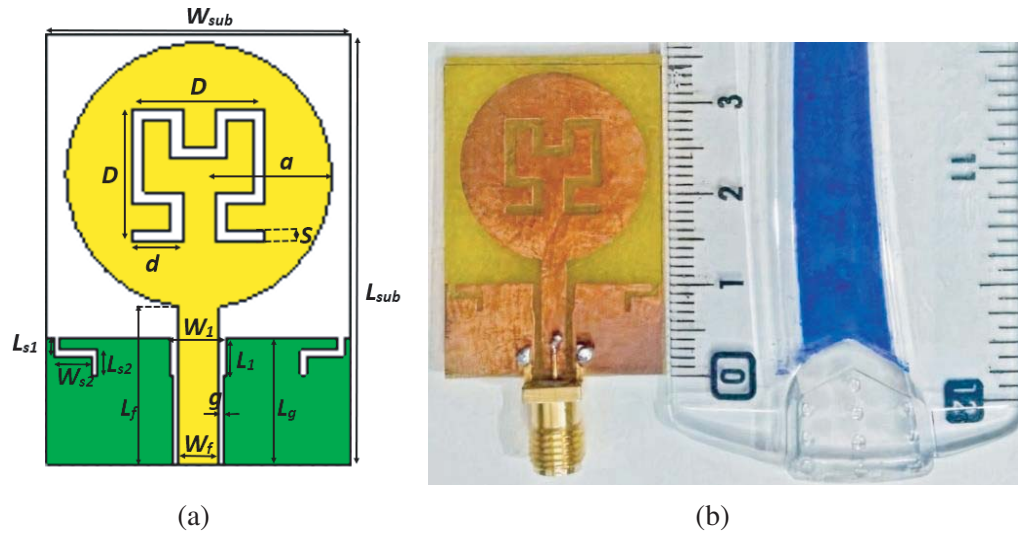
(a)   (b)

Figure 1. (a) Proposed antenna geometry; (b) Manufactured antenna prototype 1.

(a)   (b)   (c)   (d)
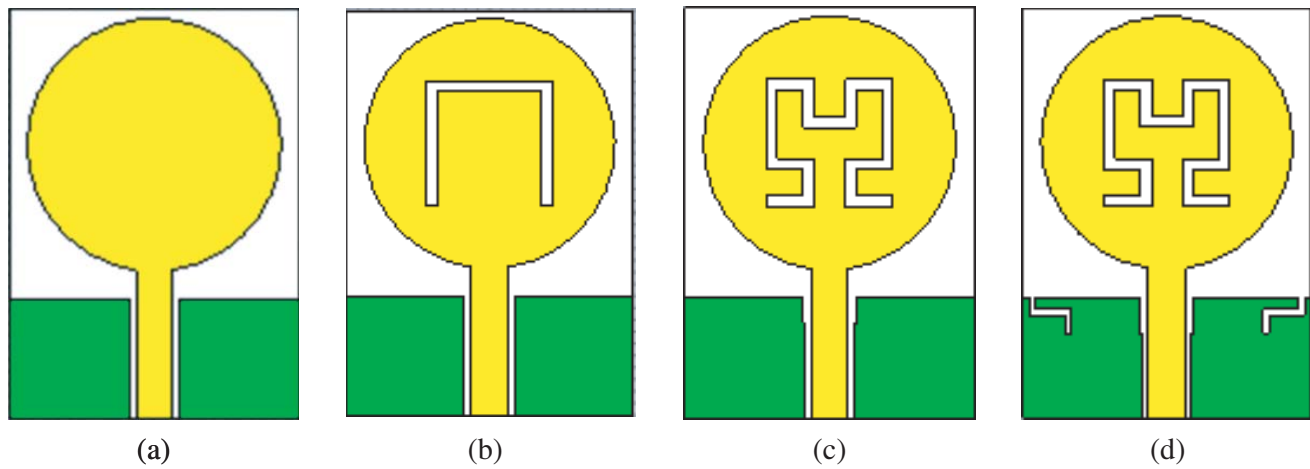
Figure 2. Design evolution process of the investigated antenna. (a) the basic antenna; (b) the first iteration; (c) the second iteration; and (d) the proposed antenna.

Table 1. Optimized parameters of the suggested antenna.

parameters	Dimensions (mm)	Parameters	Dimensions (mm)
W_{sub}	24	D	10.5
L_{sub}	34	d	3.5
h	1.6	S	0.9
a	10.5	W_{s1}	3.5
W_f	3	L_{s1}	1
L_f	12.5	L_{s2}	1.5
g	0.5	W_1	4.5
L_g	10	L_1	3

are engraved at the ground plane. The geometry evolution of the designed antenna is presented in the following subsections.

Figure 2(a) depicts the first phase in the design process of the proposed antenna. A circular radiator powered by a CPW feed line was used as a reference antenna. Using the cavity model, the circular radiator radius was calculated by employing Equations (1)–(4) [26]. The resonant frequency of circular microstrip patch antenna can be determined by:

$$f_r = \frac{cX_{np}}{2\pi a_{eff}\sqrt{\varepsilon_r}} \tag{1}$$

c: The light speed in free space, ε_r: The relative permittivity, X_{np}: The zeros of the derivative of the Bessel function Jn(x) of order n. For the mode TM11, $X_{11} = 1.84118$.

a_{eff}: The effective radius of the patch, given by:

$$a_{eff} = a \left[1 + \frac{2h}{\pi\varepsilon_r a} \left(\ln\left(\frac{\pi a}{2h}\right) + 1.7726 \right) \right]^{\frac{1}{2}} \tag{2}$$

Since the patch's effective and physical radii are nearly equal, Equation (2) may be used to calculate the real radius, which is provided by Equation (3):

$$a = \frac{F}{\left[1 + \frac{2h}{\pi\varepsilon_r F} \left(\ln\left(\frac{\pi F}{2h}\right) + 1.7726 \right) \right]^{1/2}} \tag{3}$$

where h is the height of the substrate and presented in centimeters, and F is expressed by Equation (4):

$$F = \frac{8.791 \times 10^9}{f_r\sqrt{\varepsilon_r}} \tag{4}$$

The basic circular microstrip antenna provides a single resonant frequency at $4.5\,\text{GHz}$ with a $-10\,\text{dB}$ bandwidth from $3.89\,\text{GHz}$ to $5.09\,\text{GHz}$.

Antenna 2 (Fig. 2(b)) structure is achieved by inserting an inverted U in the circular radiator slot as Hilbert fractal's first iteration.

David Hilbert, a German mathematician, described the Hilbert curve in 1891 [27]. The construction procedure of the Hilbert fractal structure is given in Fig. 3. The width of the Hilbert fractal segments and the line width are represented by S and D, respectively. The Hilbert fractal segment length is expressed by Equation (5):

$$D_n = \frac{D_{n-1}}{3} \tag{5}$$

The Hausdorff dimension is given by Equation (6) [27]:

$$d = \frac{\ln(n)}{\ln(R)} = 2 \tag{6}$$
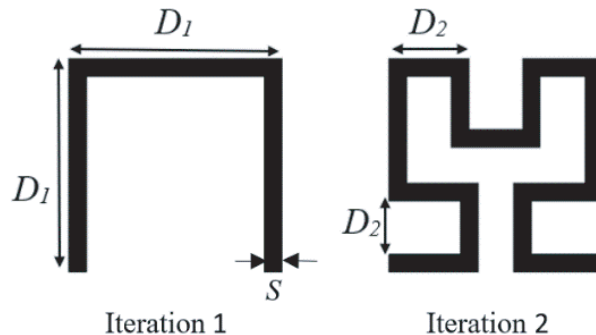
Figure 3. The first and second Hilbert fractal structure iterations.

where n and R denote the number of copies and the reduction factor, respectively.

The antenna provides two bandwidths, the first band from 3 to 3.35 GHz centered around 3.25 GHz and the second band from 3.7 to 6.92 GHz resonating at 4.4 GHz and 6.23 GHz.

In order to shift the operating bands to a lower frequency while maintaining a compact size, the second iteration of the Hilbert fractal slot is loaded into the circular radiator, and a rectangular slot of size $W_1 \times L_1$ is loaded in the ground plane as presented in Fig. 2(c). It provides two bands, 2.39–2.47 GHz and 3–6.15 GHz.

The designed antenna's final geometry is depicted in Fig. 2(d). It is obtained by inserting slots in the ground plane. This structure allows to ameliorate the antenna's impedance matching and increase the bandwidth of the second band. Moreover, the simulated S_{11} of the several steps of the developed antenna's design process is depicted in Fig. 4. The designed antenna can successfully provide two bands, 2.39–2.47 GHz and 3–6.4 GHz.
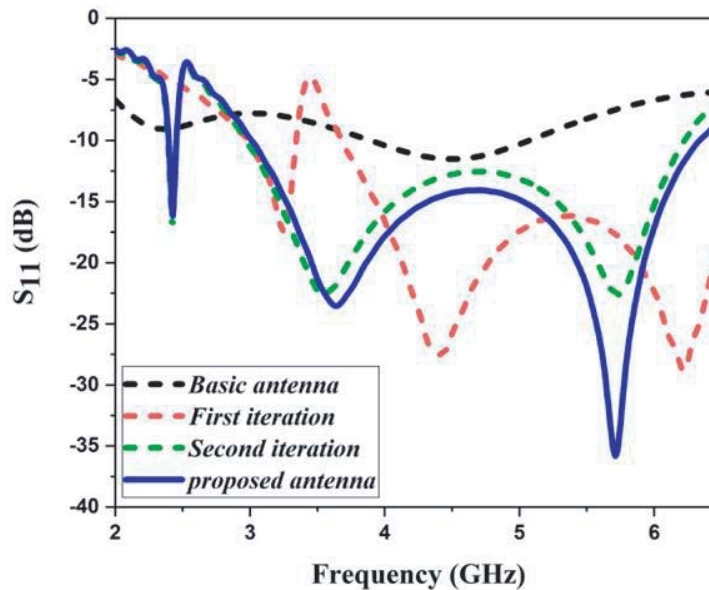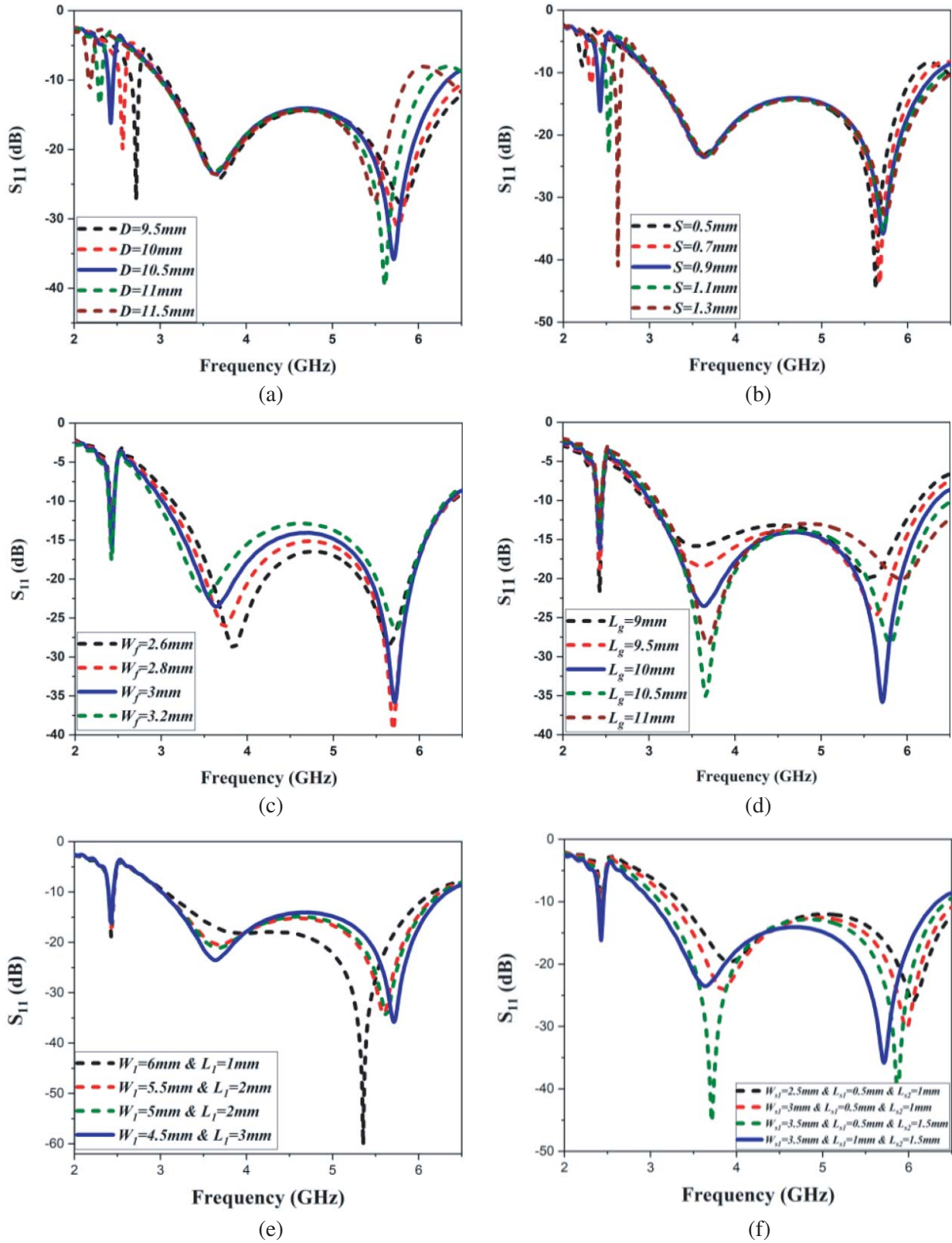

Figure 4. Variation of the reflection coefficient S_{11} for the stepwise evolution of the designed dual band antenna.

3. PARAMETRIC INVESTIGATION

The effects of several dimensional parameters on resonant frequencies, bandwidth, and impedance matching properties were studied in this section through a detailed parametric investigation. Since the Hilbert slot is mainly responsible for generating dual-band modes to obtain the requisite operating band, its dimension significantly influences antenna performance and is examined. Simultaneously, the influence of feed line, ground plane size, and DGS slots is evaluated.

The simulated S_{11} with varied values of Hilbert slot length D is shown in Fig. 5(a). The increase in the length D enhances the second bandwidth from 3–5.55 to 3–6.43 GHz, with two resonant frequencies, 3.6 and 5.8 GHz, while the first operating frequency increases from 2.2 to 2.7 GHz. It can be demonstrated that a length of 10.5 mm can provide a greater S_{11} value.

Figure 5(b) depicts the effect of S on the S_{11}. It can be claimed from the plot that the value of S highly influences the first operating frequency. And the increment of the value of S shifts the first resonant frequency from 2.25 to 2.8 GHz. On the other hand, the decrement of the value of S decreases the impedance bandwidth of the second band from 3–6.45 GHz to 3–5.7 GHz. The value of S is taken as 0.9 mm to prove the greater performances in terms of resonant frequency, operating bands, and reflection coefficient impedance matching.

Figure 5. The effects of (a) D; (b) S; (c) W_f; (d) L_g; (e) W_1 & L_1; (f) W_{s1} & L_{s1} & L_{s2} on the reflection coefficient S_{11}.

Figure 5(c) illustrates the simulated S_{11} with several values of feed line width W_f. By varying W_f from 2.6 to 3.2 mm, the second band is increased from 3.4–6.4 GHz to 3–6.43 GHz, while the first band is unchanged with the variation of the feedline width. It can be claimed from the figure that the value $W_f = 3$ mm exhibits the best performances in terms of bandwidth and impedance matching.

Figure 5(d) displays the variation of the S_{11} with different values of the ground plane length L_g (9, 9.5, 10, 10.5, and 11 mm). It can be revealed from the plot that the first resonant frequency is unaffected by the value of L_g. On the other hand, the increase in L_g increases the bandwidth of the second band from 3–5.7 GHz to 3–6.4 GHz. Furthermore, it can be noticed from the figure that the value $L_g = 10$ mm provides a good impedance matching in the operating frequencies 3.6 and 5.8 GHz.

The effect of the ground slot width and length, W_1 and L_1, on the impedance bandwidth is seen in Fig. 5(e). The increase in the width W_1 from 1 to 3 mm and the decrease in the length L_1 from 6 to 4.5 mm improve the impedance bandwidth of the second band from 3.05 to 3.4 GHz, and the third resonant frequency shifts from 5.6 to 5.8 GHz. The slot's optimum width and length are 4.5 mm and 3 mm, respectively, and the antenna attains the desired bands while maintaining good impedance matching.

The DGS slots are introduced in the ground plane. A simple parametric investigation of the DGS slot width and lengths, W_{s1}, L_{s1}, and L_{s2}, respectively, has returned us to the results shown in Fig. 5(f). The increment of W_{s1}, L_{s1}, and L_{s2}, from 2.5 to 3.5 mm, from 0.5 to 1 mm, and from 1 to 1.5 mm, shifts the upper band from 3.5–6.62 GHz to 3–6.4 GHz. In contrast, the lower band is unchanged. The DGS slots with $W_{s1} = 3.5$ mm, $L_{s1} = 1$ mm, and $L_{s2} = 1.5$ mm are optimal for achieving the requisite band of WLAN and WiMAX applications.

4. RESULTS AND DISCUSSIONS

4.1. Reflection Coefficient Results

The structure of the developed miniaturized monopole antenna is manufactured, and the S_{11} is measured using E5071C VNA to validate the simulated results experimentally. Fig. 6 illustrates the variation of the reflection coefficients S_{11} acquired by simulation and measurement versus frequency. According to measurement results, the designed antenna presents two bands of 2.39–2.47 GHz and 3–6.32 GHz, with resonance frequencies of 2.45, 3.6, and 5.7 GHz, respectively. The suggested antenna offers two bands, which shield WiMAX and WLAN bands. The simulation and measurement results are in greater
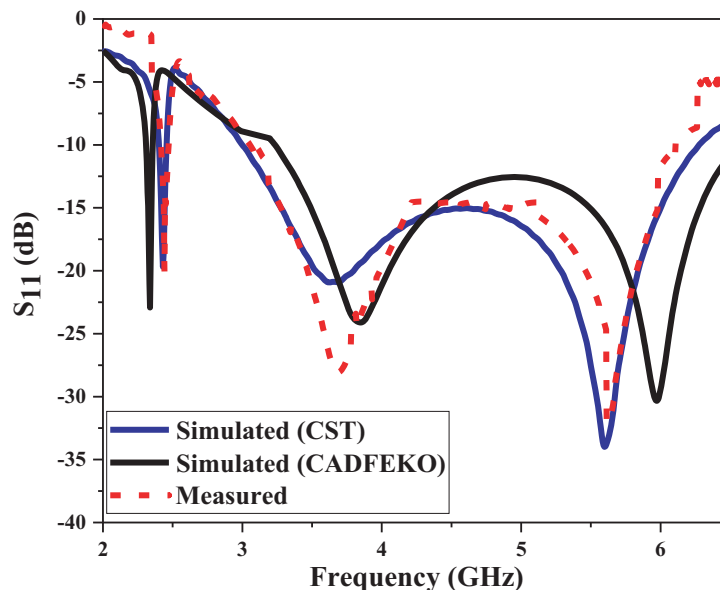

**Figure 6.** Measured and simulated reflection coefficient S_{11}.

agreement. The bands are slightly shifted in the measured results, possibly due to various factors, including manufacturing tolerance and the influence of SMA connector soldering.

4.2. The Surface Current Distribution

To better comprehend and evaluate the proposed antenna's resonant modes, the current distribution surface of the developed antenna is displayed in this section. At 2.45 GHz, the current density is highly concentrated on the feed line and surrounding the Hilbert slot, as shown in Fig. 7(a). As a result, the Hilbert fractal slot is responsible for the band around 2.45 GHz. As depicted in Fig. 7(b), the current density is higher in the feed line and ground plane at 3.6 GHz which signifies that the coupling between the feed line and ground plane produces the second band. The highest surface current is concentrated on the circular radiator, feed line, ground plane, and around the DGS slots as the frequency increases at 5.8 GHz in Fig. 7(c). The DGS slots extend the second frequency band.

(a)   (b)   (c)
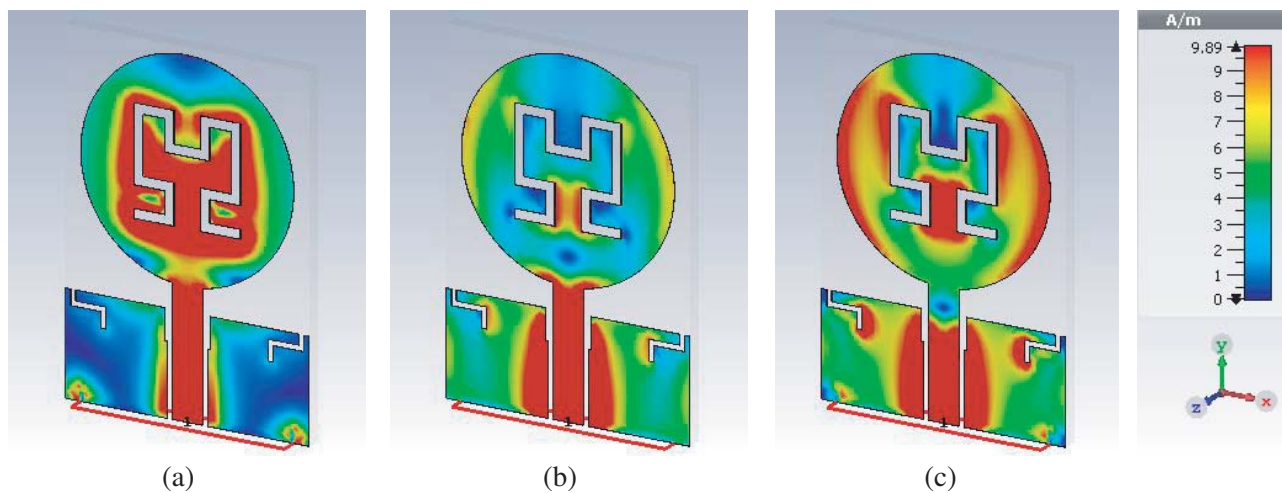
Figure 7. Current distribution of the designed antenna at (a) 2.45 GHz; (b) 3.6 GHz; (c) 5.8 GHz.
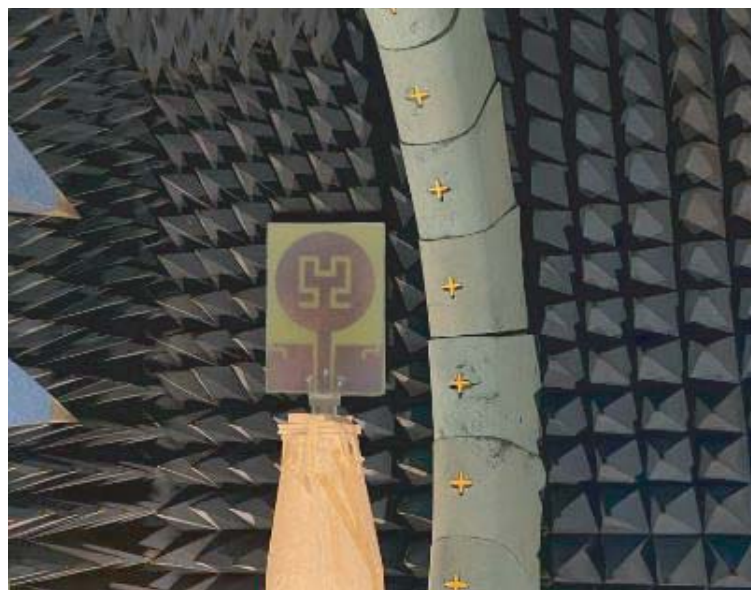
**Figure 8.** Setup for measuring radiation pattern and gain.

4.3. Radiation Pattern Results

Figure 8 depicts the radiation pattern and gain measurement setup. The radiation pattern is evaluated in an anechoic chamber operating in the frequency range of 0.5 to 40 GHz which is used to measure the radiation pattern. We have a suggested manufactured antenna in the far field evaluation chamber, and radiofrequency (RF) absorbers are employed to absorb RF signals from the antenna inside the chamber. Fig. 9 depicts the measurement results of the radiation pattern along with the simulation results acquired
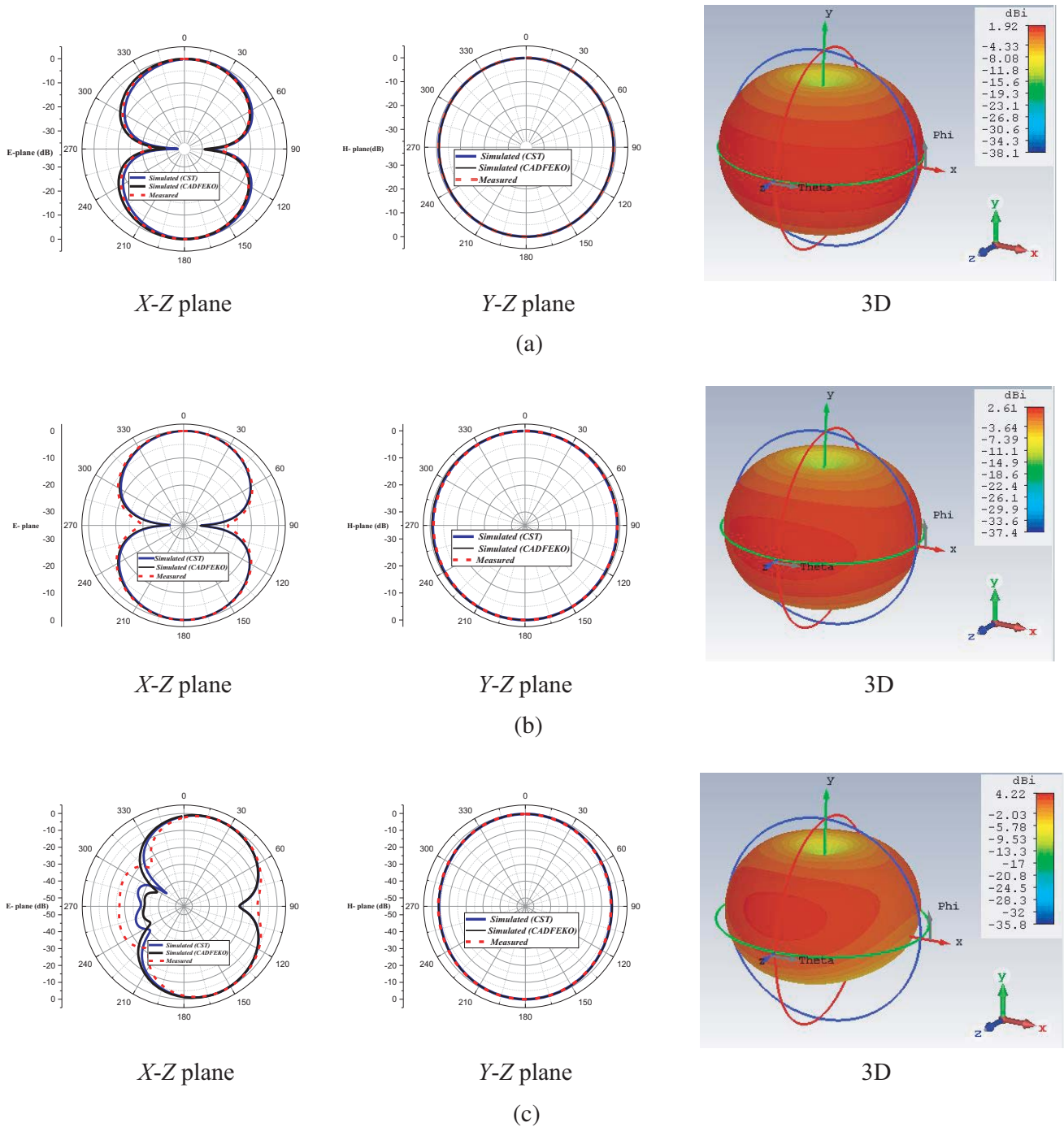
Figure 9. Measured and simulated normalized radiation patterns and 3D radiation patterns at (a) 2.45 GHz; (b) 3.6 GHz; (c) 5.8 GHz.

by CST MWS and CADFEKO solvers and the 3D radiation pattern at the operating frequencies 2.45, 3.6, and 5.8 GHz. The figures show that the obtained E- and H-planes radiation patterns are omnidirectional. Fig. 10(a) illustrates measured and simulated gains of the designed antenna, while the measured and simulated radiation efficiencies acquired by CST MWS are illustrated in Fig. 10(b). It is worth mentioning that this antenna performs well with regard to the gain and radiation efficiency. The designed antenna's gain increased to 1.8 dBi for the first band, and the radiation efficiency reached its most significant value of 96%. The gain then climbs to 4.2 dBi in the upper band, with a maximum radiation efficiency of 97%. At the operational frequencies of 2.45/3.6/5.3 GHz, the antenna provides significant gains and radiation efficiencies of 1.7/2.7/4.02 dBi and 97/95/96%, respectively. The different simulated and experimental results are illustrated in Table 2.
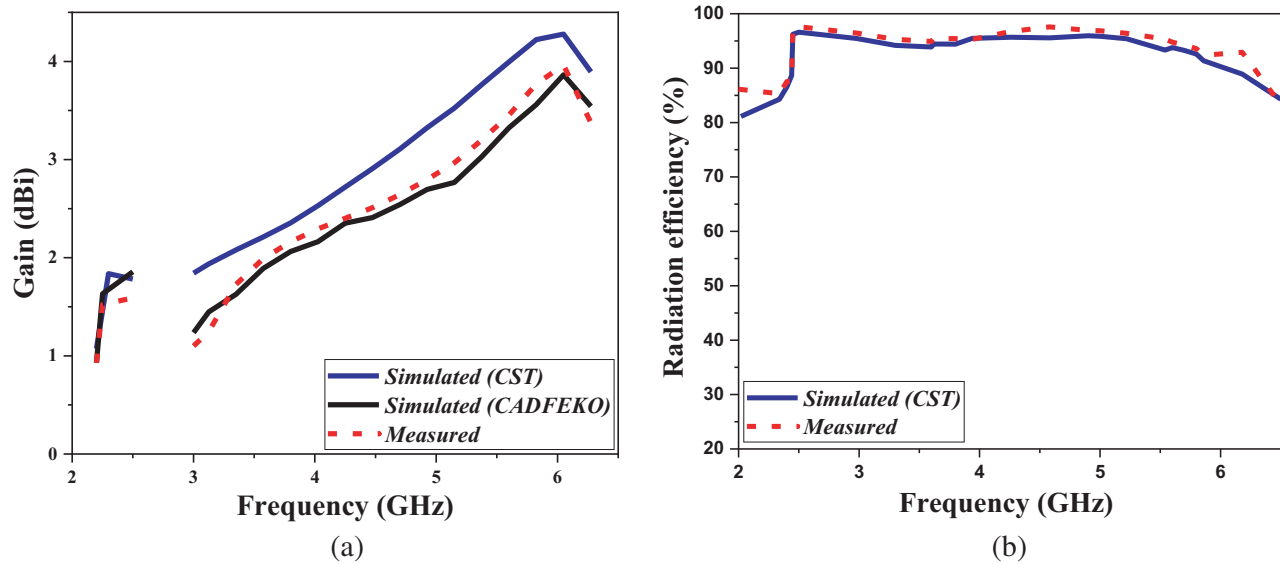
Figure 10. Measured and simulated (a) gain; (b) radiation efficiency.

Table 2. Summary of the designed antenna's simulation and experimental results.

	f_r (GHz)	S_{11} (dB)	Frequency range (GHz)	Impedance bandwidth (GHz)	Gain (dBi)
Simulation (CST)	2.45 3.6 5.8	−16 −22 −36.5	2.4–2.47 3–6.4	0.07 3.4	1.8, 2.4 4.15
Simulation (CADFEKO)	2.35 3.8 5.9	−23 −16 −28.4	2.312–2.38 3.17–6.42	0.068 3.25	1.5 1.98 3.95
Measurement	2.45 3.6 5.7	-20 -27 -32.5	2.4–2.47 3–6.32	0.07 3.32	1.7 2.1 4.02

To illuminate the features of the designed antenna, Table 3 compares the size and performance of this antenna to those reported in the literature. The developed antenna is smaller than those presented in [13–24]. Moreover, these antennas did not shield all the WLAN and WiMAX bands. The antennas reported in [13] and [16], and [19] provided a higher gain, but they had a narrow bandwidth and did

Table 3. Comparison with previous studies.

REF	Size (mm³)	Type of substrate	Bandwidth (GHz)	Resonant frequency (GHz)	Gain (dBi)	Key Design Features
[13]	60×60×1.6	FR-4	0.108, 0.108, 0.142	3.18, 4.31, 6.42	3.18, 4.31, 6.42	Circular SRR Loaded Fractal Geometry
[14]	50×50×1.5	FR-4	0.012, 0.0529, 0.0529	1.2, 2.4, 5.6	NA	Defected ground structure
[19]	60×50×1.6	FR-4	0.14, 0.18, 0.20	1.7, 3.39, 5.38	2.22, 5.18, 1.38	Two F-shaped resonator
[21]	57×31.2×1.6	FR-4	0.3, 0.9, 0.85	2.45, 3.5, 5.5	1.19, 1.59, 2.39	asymmetric E-CRLH unit cells,
[23]	30×50×1.6	FR-4	0.22, 0.13, 0.17	3.5, 4.1, 5.6	1.24, 0.62, 0.69	Triangular SRR resonator
[24]	30×54×1.6	FR-4	0.1, 3	2.45, 6	NA	dual-spectrum split-ring resonator
Proposed antenna	**24×34×1.6**	**FR-4**	**0.07, 3.32**	**2.45, 3.6, 5.7**	**1.7, 2.1, 4.02**	**Hilbert fractal slot and DGS**

not cover the band around 2.4 GHz and 3.5 GHz, respectively. The antennas introduced in [14, 23] had a large size, and they provided a narrow bandwidth and did not shield all the WLAN and WiMAX bands. The antennas introduced in [20] and [22] had a low gain in comparison to the developed antenna. Hence, the suggested antenna's significant advantages are reduced size, manufacturing simplicity, dual-band characteristic with three resonant frequencies, and high gain. As a result the designed antenna is an appropriate structure for WLAN and WiMAX applications.

5. CONCLUSION

A novel compact dual-band monopole antenna with Hilbert fractal slot and DGS is introduced in this work. The proposed antenna is constructed on an FR-4 epoxy substrate of size $24 \times 34 \times 1.6 \, \text{mm}^3$. Because of its planar structure, it is simple to fabricate at low cost. Additionally, the experimental results show that the designed antenna provides two bands, the lower band 2.39–2.47 GHz centered at 2.45 GHz and the upper band 3–6.32 GHz with two operating frequencies 3.6 and 5.7 GHz. These bands are suitable for WiMAX bands (2.3/2.5/3.3/3.5/5/5.5 GHz) and WLAN bands (2.4–2.5/3.6/4.9–5.9 GHz). At the resonant frequencies 2.45/3.6/5.7 GHz, the investigated antenna achieves acceptable peak gains of 1.7/2.1/4.02 dBi, as well as radiation efficiencies of 97/95/96%. Hence, the H- and E-planes radiation patterns of the suggested antenna are omnidirectional.

REFERENCES

1. Kunwar, A., A. K. Gautam, B. K. Kanaujia, and K. Rambabu, "Circularly polarized D-shaped slot antenna for wireless applications," *Int. J. RF Microw. Comput. Aided Eng.*, Vol. 29, No. 1, e21498, Jan. 2019.

2. Ghaffar, A., A. Altaf, A. Aneja, et al., "A frequency reconfigurable compact planar inverted-F antenna for portable devices," *International Journal of Antennas and Propagation*, Vol. 2022, 7239608, Jan. 2022.

3. Cao, Y. F., S. W. Cheung, and T. I. Yuk, "A multiband slot antenna for GPS/WiMAX/WLAN systems," *IEEE Trans. Antennas Propagat.*, Vol. 63, No. 3, 952–958, Mar. 2015.

4. Ullah, S., S. Ahmad, B. A. Khan, and J. A. Flint, "A multi-band switchable antenna for Wi-Fi, 3G advanced, WiMAX, and WLAN wireless applications," *Int. J. Microw. Wireless Technol.*, Vol. 10, No. 8, 991–997, Oct. 2018.

5. Benkhadda, O., S. Ahmad, M. Saih, K. Chaji, A. Reha, A. Ghaffar, S. Khan, M. Alibakhshikenari, and E. Limiti, "Compact broadband antenna with vicsek fractal slots for WLAN and WiMAX applications," *Applied Sciences*, Vol. 12, No. 3, 1142, Jan. 2022.

6. Jo, S., H. Choi, J. Lim, B. Shin, S. Oh, and J. Lee, "A CPW-fed monopole antenna with double rectangular rings and vertical slots in the ground plane for WLAN/WiMAX applications," *International Journal of Antennas and Propagation*, Vol. 2015, 1–7, 2015.

7. Reha, A., A. El Amri, O. Benhmammouch, A. Oulad Said, A. El Ouadih, and M. Bouchouirbat, "CPW-fed slotted CANTOR Set fractal antenna for WiMAX and WLAN applications," *Int. J. Microw. Wireless Technol.*, Vol. 9, No. 4, 851–857, May 2017.

8. Bhowmik, A. and A. Kr. Bhattacharjee, "Design of A-shaped coaxial fed compact broadband antenna for WLAN/WiMAX/UWB lower-band applications," *Microw. Opt. Technol. Lett.*, Vol. 59, No. 4, 848–853, Apr. 2017.

9. Kunwar, A. and A. K. Gautam, "Fork-shaped planar antenna for Bluetooth, WLAN, and WiMAX applications," *Int. J. Microw. Wireless Technol.*, Vol. 9, No. 4, 859–864, May 2017.

10. Ren, W., S.-W. Hu, and C. Jiang, "An ACS-fed F-shaped monopole antenna for GPS/WLAN/WiMAX applications," *Int. J. Microw. Wireless Technol.*, Vol. 9, No. 5, 1123–1129, Jun. 2017.

11. Brar, R. S., K. Saurav, D. Sarkar, and K. V. Srivastava, "A quad-band dual-polarized monopole antenna for GNSS/UMTS/WLAN/WiMAX applications," *Microw. Opt. Technol. Lett.*, Vol. 60, No. 3, 538–545, Mar. 2018.

12. Gangwar, S. P., K. Gangwar, and A. Kumar, "Dual-band modified circular slot antenna for WLAN and WiMax applications," *Progress In Electromagnetics Research C*, Vol. 85, 247–257, 2018.

13. Kaushal, D. and T. Shanmuganantham, "Parametric enhancement of a novel microstrip patch antenna using Circular SRR Loaded Fractal Geometry," *Alexandria Engineering Journal*, Vol. 57, No. 4, 2551–2557, Dec. 2018.

14. Mabaso, M. and P. Kumar, "A microstrip patch antenna with defected ground structure for triple band wireless communications," *JCM*, 684–688, 2019.

15. Patel, R., T. Upadhyaya, A. Desai, and M. Palandoken, "Low profile multiband meander antenna for LTE/WiMAX/WLAN and INSAT-C application," *AEU — International Journal of Electronics and Communications*, Vol. 102, 90–98, Apr. 2019.

16. Park, J., M. Jeong, N. Hussain, S. Rhee, P. Kim, and N. Kim, "Design and fabrication of triple-band folded dipole antenna for GPS/DCS/WLAN/WiMAX applications," *Microw. Opt. Technol. Lett.*, Vol. 61, No. 5, 1328–1332, May 2019.

17. Ghaffar, A., W. A. Awan, N. Hussain, S. Ahmad, and X. J. Li, "A compact dual-band flexible antenna for applications at 900 and 2450 MHz," *Progress In Electromagnetics Research Letters*, Vol. 99, 83–91, 2021.

18. Yu, Z., Z. Lin, X. Ran, Y. Li, B. Liang, and X. Wang, "A novel " " pane structure multiband microstrip antenna for 2G/3G/4G/5G/WLAN/navigation applications," *International Journal of Antennas and Propagation*, Vol. 2021, 1–15, Jun. 2021.

19. Elkorany, A. S., A. N. Mousa, S. Ahmad, D. A. Saleeb, A. Ghaffar, M. Soruri, M. Dalarsson, M. Alibakhshikenari, and E. Limiti, "Implementation of a miniaturized planar tri-band microstrip patch antenna for wireless sensors in mobile applications," *Sensors*, Vol. 22, No. 2, 667, Jan. 2022.

20. Karmakar, A., R. Ghatak, D. R. Poddar, and U. Banerjee, "Complementary stacked patch antenna with fractal shape defect for wideband characteristics," *Microw. Opt. Technol. Lett.*, Vol. 56, No. 4, 944–947, Apr. 2014.

21. Chu, H. B. and H. Shirai, "A compact metamaterial quad-band antenna based on asymmetric E-CRLH unit cells," *Progress In Electromagnetics Research C*, Vol. 81, 171–179, 2018.

22. Thamil Selvi, N., P. Thiruvalar Selvan, S. P. K. Babu, and R. Pandeeswari, "Multiband metamaterial-inspired antenna using split ring resonator," *Computers & Electrical Engineering*, Vol. 84, 106613, Jun. 2020.

23. Mahendran, K., R. Gayathri, and H. Sudarsan, "Design of multi band triangular microstrip patch antenna with triangular split ring resonator for S band, C band and X band applications," *Microprocessors and Microsystems*, Vol. 80, 103400, Feb. 2021.

24. Yeboah-Akowuah, B., E. T. Tchao, M. Ur-Rehman, M. M. Khan, and S. Ahmad, "Study of a printed split-ring monopole for dual-spectrum communications," *Heliyon*, Vol. 7, No. 9, e07928, Sept. 2021.

25. Patel, U. and T. K. Upadhyaya, "Design and analysis of compact μ-negative material loaded wideband electrically compact antenna for wlan/wimax applications," *Progress In Electromagnetics Research M*, Vol. 79, 11–22, 2019.

26. Balanis, C. A., *Antenna Theory: Analysis and Design*, 4th Edition, John Wiley, 2016.

27. Hilbert, D., "Ueber die stetige Abbildung einer Line auf ein Flachenstuck," *Math. Ann.*, Vol. 38, No. 3, 459–460, Sept. 1891.